Korean J. Chem. Eng., 34(5), 1281-1293 (2017)
DOI: 10.1007/s11814-017-0064-7
pISSN: 0256-1115
eISSN: 1975-7220

INVITED REVIEW PAPER

Interfacial phenomena between conjugated organic molecules and noble metals

Ju-Hyung Kim[*,**,†]

*Department of Chemical Engineering, Ajou University, Suwon 16499, Korea
**Department of Energy Systems Research, Ajou University, Suwon 16499, Korea
(*Received 31 January 2017 • accepted 5 March 2017*)

Abstract−Understanding interfacial interaction between conjugated organic molecules and noble metals is important not only for surface science, but also in relation to organic epitaxy, the architecture of intermolecular networks or nanostructures, and organic electronics. Particularly, properties of interfacial geometric and electronic structures and their related phenomena have attracted much interest for their potential in various electronic and optoelectronic applications, and thus extensive efforts have been devoted to understand and control organic/metal interfaces. We provide an overview of interfacial phenomena between conjugated organic molecules and noble metals *via* various interactions at the organic/metal interfaces such as surface-molecule and intermolecular interactions, as well as recent progress achieved in this area.

Keywords: Organic Molecules, Organic Thin-films, Noble Metals, Organic/Metal Interfaces, Interfacial Interactions

INTRODUCTION

Conjugated organic molecules have received much attention as promising materials with high charge-carrier mobility and environmental stability for molecule-based electronics, and they present remarkable advantages compared to standard inorganic technologies such as low cost, low weight, low-temperature process, and mechanical flexibility [1-5]. Using conjugated organic molecules in electronic devices also can provide excellent controllability of geometric and electronic structures of active components which play a critical role in determining device characteristics and performance [6]. Extensive research thus has been devoted to the development and advancement of molecule-based electronics and their applications in the past few decades, which include not only organic thin-film devices such as organic light emitting diodes (OLED), organic thin-film transistors (OTFT), and organic photovoltaic (OPV), but also molecular devices at the single-molecule level [2, 3,5,7-18].

In recent years, it has been recognized that interfacial contacts between conjugated organic molecules and metal electrodes play important roles as molecular functionality in molecule-based electronics. As shown in Fig. 1, organic/metal (O/M) interfaces are where charge transfers between active components and electrodes occur in organic thin-film devices, and such interfacial contacts

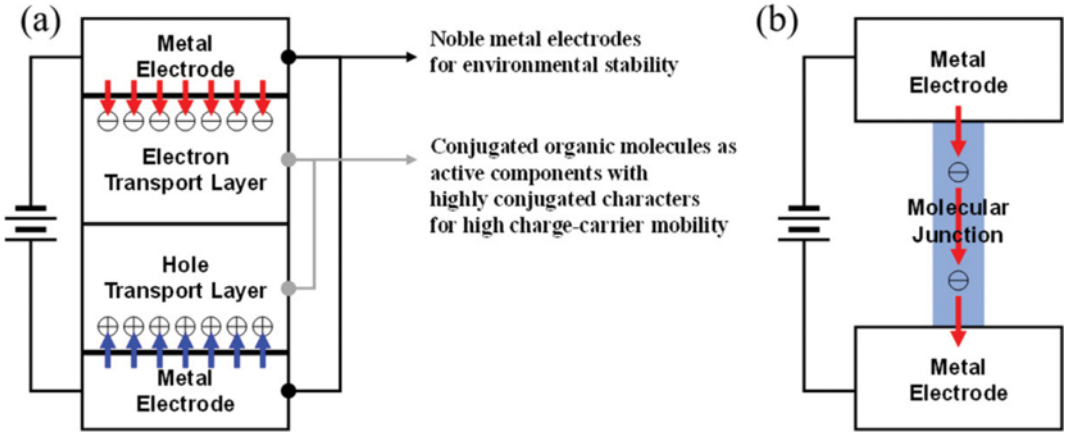

Fig. 1. Schematic illustration of charge transfers between active components and electrodes in (a) organic thin-film devices and (b) molecular junction devices.

†To whom correspondence should be addressed.
E-mail: juhyungkim@ajou.ac.kr

are also present in any persuasive models for molecular devices [6]. In addition, balancing of various interactions at the O/M interfaces (i.e., surface-molecule and intermolecular interactions) is important in organic epitaxy and the architecture of intermolecular networks or nanostructures in reference to size and structural control of the system [19-21]; and the molecular registry on a metal surface governed by interfacial interactions has strong correlation with the subsequent film growth and its electronic structure [22, 23]. Therefore, how to understand and control interfacial interactions and their related phenomena is one of today's challenging issues not only in the field of surface science, but also in various fields of science and engineering in relation to organic electronics.

Noble metals, represented by gold (Au), silver (Ag), and copper (Cu), have been widely used as electrodes in molecule-based electronics owing to their chemical inertness, different from other transition metals which cause oxidation or instability [2,24,25]. The use of noble metal substrates also facilitates changing surface-molecule interactions corresponding to work-function of metal, surface lattice, and surface templating effect. Moreover, since conjugated organic molecules normally lie flat on noble metal surfaces, intentional tuning of intermolecular interactions at the O/M interfaces can be achieved by careful design of the molecules incorporating chemical properties. Accordingly, the interfaces between conjugated organic molecules and noble metals provide an excellent framework for systematic study of numerous factors involved in understanding and controlling the O/M interfaces and their related phenomena. This review thus focuses on the O/M interfaces formed with conjugated organic molecules and noble metals, and provides an overview of various interfacial interactions and their related phenomena as well as recent progress achieved in this area from

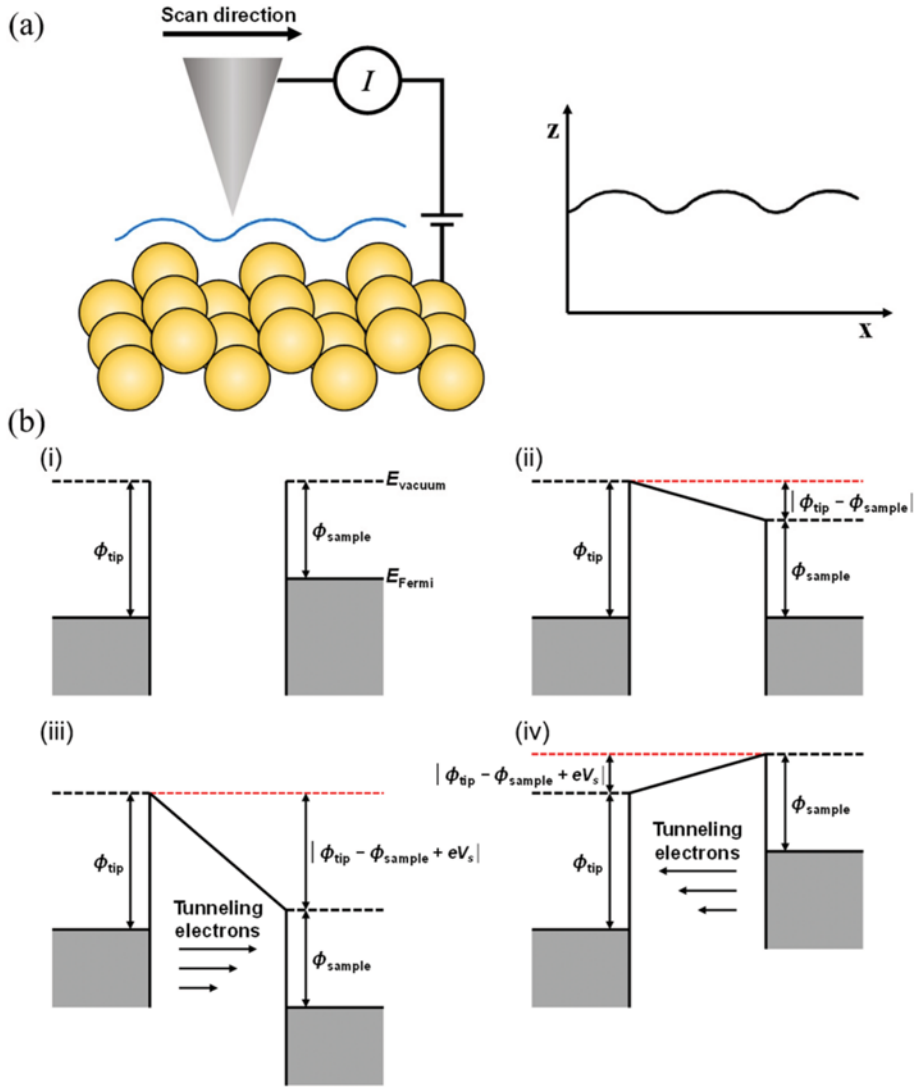

Fig. 2. (a) Schematic illustration of constant current imaging mode of STM operation. A tip-sample distance is adjusted by a feedback loop during scanning, and such height adjustment of the tip is recorded. (b) Energy level diagrams for tip and sample when an appropriate voltage is applied to the sample (i.e., sample bias voltage). (i) Independent sample and tip, which are completely separated. (ii) Sample and tip at equilibrium without sample bias. (iii) For positive sample bias, electrons tunnel from tip to sample. (iv) For negative sample bias, electrons tunnel from sample to tip.

an experimental point of view. Note that theoretical modelling and computational works are now widely performed using density functional theory (DFT) to complement experimental approaches and describe interfacial phenomena in detail, even if DFT calculations considering both molecules and surfaces require significant amounts of computational resources. For additional information concerning the DFT calculations, the reader may wish to refer to other reviews [21,26,27]. This article mainly addresses surface-molecule and intermolecular interactions involved in the formation of interfacial geometric and electronic structures, based on scanning tunneling microscopy/spectroscopy (STM/STS) [28]. This review may afford not only deeper insight into the O/M interfacial structures, but also new perspectives to organic electronics using conjugated organic molecules and noble metals.

SCANNING TUNNELING MICROSCOPY AND SPECTROSCOPY

Since the IBM laboratory succeeded in the development of a scanning tunneling microscope, it has become a powerful tool for topographic imaging, spectroscopy, and their combinations [29-31]. The fundamental principle of STM operation is based on the quantum tunneling of electrons. As shown in Fig. 2, a tunneling current can flow due to the quantum tunneling effect when a sharp metal tip is brought close enough to a conducting sample surface within a separation of only a few Å range. The tunneling current can be used to probe local physical properties as well as to measure topography of the sample surface with sub-atomic accuracy.

The most widely used mode for STM operation is a constant current imaging mode. In this mode, a tip-sample distance is adjusted by a feedback loop during scanning, and the tunneling current between tip and sample is maintained at a constant set value when an appropriate voltage is applied to the sample (i.e., sample bias voltage). The sample bias voltage is normally applied within a range from a few mV to a few V while the tip is grounded. Thus, the tunneling current corresponding to the sample bias voltage typically varies from a few pA to hundreds nA, and the exponential dependence of the tunneling current on the tip-sample distance enables topographic imaging with a high spatial resolution.

When the sample bias voltage, V_s, is applied to the sample in STM operation, the energy levels of the sample shift downward or upward in energy by $|eV_s|$ corresponding to the bias polarity as shown in Fig. 2(b) [32]. Electrons tunnel into unoccupied states of the sample from the tip for positive sample bias, and from occupied states of the sample into the tip for negative sample bias. Thus, the electronic states contributing the tunneling current, I, vary with the sample bias, of which the polarity determines either occupied or unoccupied states of the sample are probed. In a spectroscopy context, a spatially resolved signal of dI/dV_s can be obtained by a lock-in amplifier technique, which is well-known as STS [33-35]. With simple assumptions, the dI/dV_s signal are simplified as follows [32]:

$$\left.\frac{dI_t}{dV_s}\right|_{V_s} \propto en_t(0)\cdot n_s(eV_s)\cdot T(eV_s, eV_s) + \int_0^{eV_s} n_t(\pm eV_s \mp E)\cdot n_s(E)\cdot \frac{dT(E, eV_s)}{dV_s} dE$$

where n_t and n_s are density-of-states (DOS) of the tip and the sample, respectively, and T is a transmission coefficient. At a fixed location of the tip, the first term of the equation reflects the local DOS (LDOS) of the sample at eV_s with respect to the Fermi level

Category	A	B	C
Adsorption Characteristics	Physisorption	Weak chemisorption (with physisorptive characteristics)	Strong chemisorption
Main Interaction	Van der Waals interaction	Certain degree of orbital hybridization or charge transfer	Covalent bonding at specific site
Mode of Epitaxy	Incommensurism (Rarely coincidence or commensurism)	Coincidence (Rarely commensurism)	Commensurism
Example of Interface	π-conjugated hydrocarbon molecules on the noblest metal surface, Au(111)	Conjugated organic molecules on clean noble metal surfaces	Conjugated organic molecules with intrinsic dipoles and/or anchoring groups on clean noble metal surfaces

Fig. 3. Three types of interfaces between conjugated organic molecules and noble metals classified in terms of surface-molecule interaction strength.

(E_F), and a variation in T corresponding to V_s becomes smooth and monotonic. Therefore, the dI/dV_s signal as a function of V_s can be directly interpreted as overall structure of the LDOS of the sample.

SURFACE-MOLECULE INTERACTIONS

Surface-molecule interactions are normally reflected in local adsorption geometry and its electronic structure. When a conjugated organic molecule is brought into contact with a noble metal surface, the adsorption process may involve several interfacial interactions and effects (e.g., van der Waals (vdW) interaction, polarization of the electron density, partial charge transfer through covalent bonding, and other chemical interactions via orbital hybridization) [6,19-23,36-40].

1. Adsorption Geometry

To understand the adsorption process relevantly, the O/M interfaces are generally classified by the strength of surface-molecule interactions, and cases of conjugated organic molecules on noble metal surfaces are also categorized in the same manner as described in Fig. 3 [22,41,42].

First, it has been commonly considered that conjugated organic molecules without any functional groups which might chemically interact with noble metals, i.e., π-conjugated hydrocarbon molecules, physisorb on the noblest Au surface without significant electronic coupling (categorized into A in Fig. 3) [19,24,36,42]. Note that the close-packed (111) facet is the most thermodynamically stable and chemically inert surface of Au, and thus the noblest Au surface normally corresponds to the Au(111) surface [43]. Highly delocalized highest occupied molecular orbital (HOMO) and lowest unoccupied molecular orbital (LUMO) states of the conjugated molecule are basically spread throughout the entire molecular structure, and the noble metals with full d bands show lower reactivity as compared with other transition metals [24]. Particularly on the Au(111) surface, both HOMO and LUMO states of π-conjugated hydrocarbon molecule rarely give origin to charge transfer with the surface owing to high chemical inertness of the Au(111) surface and its highest work-function (~5.2 eV) [44,45]. Therefore, the adsorption process of π-conjugated hydrocarbon molecules onto the noblest Au surface is mainly governed by vdW interactions in a flat-lying manner, and the π-states of molecules are well-preserved and accompanied with a small degree of molecular level broadening. It implies that a variation in adsorption energy corresponding to various molecular orientations is normally too small to determine specific adsorption geometry under these conditions, due to a shallow vdW potential minimum [46]. With those reasons, incommensurate or coincident growth of molecular layers is generally observed in most cases of the A category, and lateral interactions between adsorbates in the system should be considered to determine the mode of quasi-epitaxy as will be discussed below in relation to intermolecular interactions and further reviewed elsewhere [21,46]. Note that the herringbone reconstruction of the Au(111) surface is not seriously affected by physisorbed adsorbates, and rather plays a role as a template, which can limit the size of molecular domains [47-51]. Fig. 4(a) shows that the Au herringbone reconstruction is still present at about one monolayer (ML) coverage of benzene (~0.99 ML) on the Au(111) surface [52], indicating that surface-molecule interactions are weak and mostly based on the vdW interactions. In addition, as experimental and theoretical techniques have progressed, the existence and contribution of valid surface-molecule interactions other than vdW interactions in such physisorptive systems have been questioned and probed [25,53-55]. Various π-conjugated hydrocarbon molecules, such as benzene [52,56], pentacene [23,53,57], perylene [58,59], coronene [58], and dehydrobenzo[12]annulene (DBA) [60], on the Au(111) surface have been studied thus far, indicating that the pillow effect, i.e., polarization effect of electron density at the O/M interface, contributes to the formation of interface dipoles with the vdW adsorption characters [22,61,62]. DBA interestingly shows a specific adsorption configuration even on the noblest Au(111) surface in low-temperature experiments (see Fig. 4(b)), suggesting that small contribution of very (and normally negligible) weak electronic coupling between molecular π-states and electronic states of the Au(111) surface can play a crucial role in constraining adsorption geometry even in the archetypal adsorption system of category A [60].

Secondly, many types of conjugated organic molecules, which normally contain polar groups, show some extent of orbital hybridization with noble metal surfaces, i.e., formation of mixed molecule-metal states, even though covalent bonding cannot be distinctly claimed (categorized into B in Fig. 3) [42]. Note that this category B also includes π-conjugated hydrocarbon molecules on noble metal surfaces other than the Au(111) surface. In this category, determination of specific adsorption geometry is relatively clearer than the category A. Representative instances which fit into this category are 3,4,9,10-perylene-tetracarboxylic acid dianhydride (PTCDA) on the Ag(111) surface, benzene on the Cu(100) surface, and pectacene on the Cu(111) surface [25,63-68]. In this category, the features corresponding to HOMO and LUMO states of adsorbed molecule are commonly broadened in the energy region close to the E_F of substrate. Such adsorption characters mainly originate from the hybridization of LUMO state, which becomes partially occupied via static electron transfer from metal to molecule. Thus, the LUMO is the molecular state most closely connected to the metallic charge reservoir of the substrate. Particularly in the case of PTCDA/Ag(111), M. Eremtchenko et al. revealed that it can be experimentally probed which part of the adsorbed molecule is coupled to the metallic charge reservoir most strongly (that is, which part of the molecule plays the predominant role in chemical interaction with the substrate) because the metal electrons respond to the redistribution of the electron density in the LUMO modulated by a vibrational excitation (see Fig. 4(c)) [64].

Finally, adsorption of conjugated organic molecules which contain anchoring groups onto noble metal surfaces is classified as strong chemisorption via plain covalent bonding (categorized into C in Fig. 3) [37,42]. In this category, it is normally possible to describe the growth mode of molecular layers as point-on-point coincidence (i.e., commensurism) with the substrates, which means that each primitive lattice vector of molecular layers is an integer multiple of an identically oriented substrate lattice vector [46]. Formation of organic self-assembled monolayers (SAMs) via covalent Au-thiol bonds is the most representative instance of this category [69,70], and the adsorption energy (a few eV) is much larger in

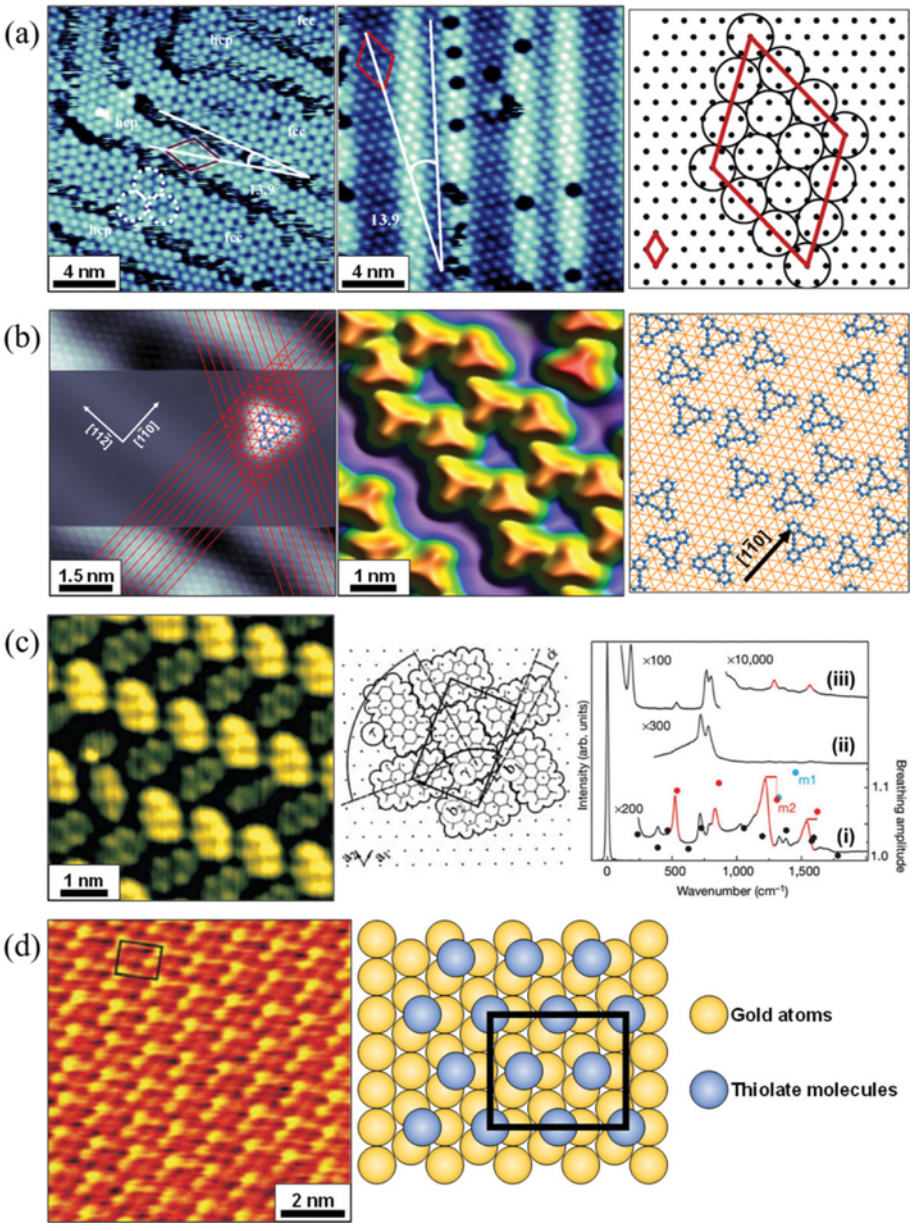

Fig. 4. (a) STM images of 0.9 ML (left) and 0.99 ML (middle) of benzene on Au(111), and model structure of the benzene monolayer over the hcp region of Au(111) (right). Red rhombus indicates the unit cell of the structure. Reprinted with permission from ref. 52; Copyright (2004) American Chemical Society. (b) STM image of isolated DBA molecule on Au(111) obtained by spatially varying the tunneling conditions (left), high-coverage STM image of DBA/Au(111) (middle), and corresponding model structure (right). Reprinted with permission from ref. 60; Copyright (2012) American Institute of Physics. (c) STM image of the herringbone phase layer of PTCDA on Ag(111) (left), corresponding model structure (middle), and electron energy-loss spectra for PTCDA and perylene on Ag(111) (right). Red peaks in (i) correspond to a particular set of Raman enhanced modes at 0.3 ML of PTCDA, which are not observed in (ii) low-temperature experiments at 100 K. Perylene shows only slight activation of two Raman modes on Ag(111) as indicated in (iii). Circles indicate the breathing amplitude of the central carbon ring of PTCDA, of which six modes are particularly large (red and blue circles). Four breathing modes indicated with red circles coincide with the Raman enhanced modes to which the metal electrons strongly respond. Reprinted with permission from ref. 63; Copyright (1998) Elsevier and ref. 64; Copyright (2003) Nature Publishing Group. (d) STM image of organic self-assembled monolayer composed of decanethiol ($C_{10}H_{21}SH$) on the Au substrate (left), and corresponding model structure (right). Black box indicates the unit cell of the structure. Reprinted with permission from ref. 73; Copyright (2009) Elsevier.

comparison with the physisorptive systems [71,72]. In addition, differently from the other categories A and B, the adsorption process in a planar fashion is not necessary any longer due to the anchoring groups onto the noble metal surfaces. The adsorbates can stand in an upright direction in some cases such as organothiol on the Au(111) surface (see Fig. 4(d)) [73].

Note that adsorption geometry can be determined by high resolution microscopy, which is accompanied with density functional theory (DFT) calculations in many cases. For the direct site-determination of an adsorbate, high sensitivity and wide dynamic range of microscopy are required, because simultaneous observations of the substrate corrugation and the position of molecule are necessary. The change in the height profile owing to the adsorbate can be as large as several angstroms (Å), but the corrugation associated with a close-packed metal surface is only of the order of 0.001-0.01 Å [60,74-76].

2. Electronic Structure

Physisorption of conjugated organic molecules on noble metal surfaces (in the categories A and B) mainly occurs via the vdW interactions [36]. In this case, the valence electron distribution in the adsorbate is polarized toward the metal surface, and it mainly originates from the image force and the exchange-correlation force [6,40]. Valence electrons of the molecule, which stay away from each other according to the Pauli exclusion principle, are stabilized by the image charges near the metal surface, and thus surrounded by the exchange-correlation holes. Such attractive interactions lead to lowering the energy of the system, and the polarization effect of the adsorbate is accompanied with redistribution of the surface electron density [41,62,77,78]. Upon physisorption of the adsorbate on the noble metal surface, the spill-out electron density of the metal surface is pushed back into the metal substrate to a certain degree, inducing redistribution of the electron density of the metal surface (see Fig. 5(a)). However, if the adsorbate is too close to the metal surface, the repulsive interaction between the valence electrons of the adsorbate and the redistributed spill-out electron density from the metal surface starts to dominate over the attractive interaction. The balance of these attractive and repulsive interactions consequently determines a shallow potential well from the surface (a few Å from the surface) and an optimal interfacial distance between the physisorbed adsorbate and the noble metal surface [60]. In the category B, unoccupied molecular states such as LUMO+n (n=0, 1, 2, …), which are not directly involved in the physisorption process of the category A, can be strongly coupled to the metal surface through extensive wave function mixing, allowing chemisorptive properties as well.

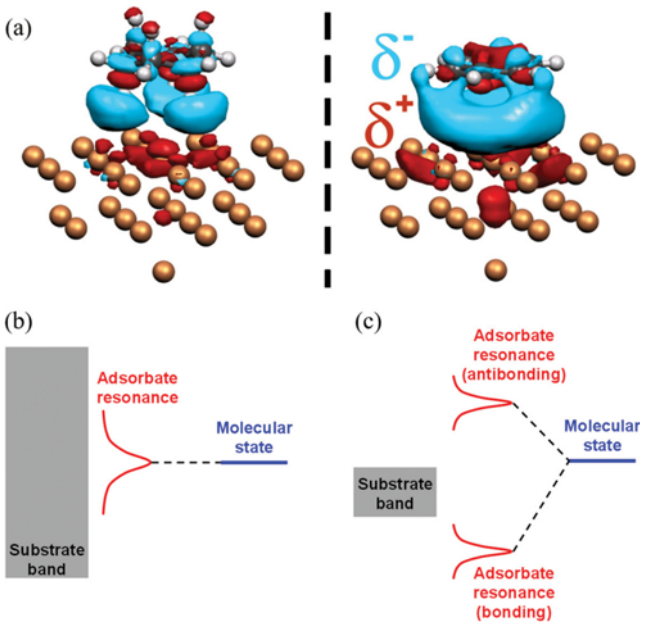

Fig. 5. (a) Charge density difference maps of cyclohexane (left) and benzene (right) on the identical Cu clusters (32 atoms), showing redistribution of the surface electron density. The adsorbates push the spill-out electron density of the metal surface. Reprinted with permission from ref. 62; Copyright (2005) American Institute of Physics. (b), (c) Schematic illustration of chemisorption. Based on the Newns-Anderson model, discrete molecular states interact with (b) broad substrate band (larger than V_{ET}) and (c) narrow substrate band (smaller than V_{ET}).

Chemisorption significantly involves chemical interactions between the adsorbate and the substrate (in the categories B and C) [37,79,80]. Based on the Newns-Anderson model [81], a discrete adsorbate state, |a>, interacts with a continuum of Bloch states of the substrate (i.e., a substrate band), |k>. According to this model in consideration of major contribution factors, the shifts of adsorbate states due to the image interaction of physisorption can be neglected, and the total Hamiltonian ($\hat{H}$) is simplified as $\hat{H}_M+\hat{H}_S+\hat{V}_{ET}$, where $\hat{H}_M$ and $\hat{H}_S$ are Hamiltonians for the isolated molecule and the substrate, respectively, and $\hat{V}_{ET}$ is the coupling term of electron transfer between the discrete molecular state and the substrate electronic continuum. The coupling term is responsible for broadening of molecular resonance, which is a mixture of the |a> and |k> states. When the coupling is relatively weak as in the category B, the coupling energy (V_{ET}) is smaller than the width of the substrate band, and the projected DOS (PDOS) of the molecular resonance onto the adsorbate has a Lorentzian shape with the width, Γ (see Fig. 5(b)). Here Γ can be determined by a direct measurement of lifetime of transient molecular resonance (τ) based on the uncertainty principle (i.e., $\Gamma \approx \hbar/\tau$) [6,40]. On the other hand, for strong chemisorption of the category C, the coupling energy (V_{ET}) is larger than the width of the substrate band. In this case, the molecular state interacting with the metal surface splits into bonding and antibonding states as shown in Fig. 5(c).

The overall electronic states of organic thin films or molecular layers on noble metal surfaces will be discussed in the later section, "electronic states at organic-metal interfaces".

LATERAL INTERMOLECULAR INTERACTIONS

Structuring of organic thin films or molecular layers, which is an excellent way of modifying the properties of metal surfaces, has been proposed as active elements in molecule-based electronic applications such as memory devices [82-89]. In the formation of such molecular layers, lateral interplay between molecules (i.e., intermolecular interactions in a lateral direction) is dominant as well as the surface-molecule interactions in an upright direction. Thus, ordering of molecules within molecular domains on noble metal surfaces is practically governed by self-assembly processes through balancing of molecule-molecule and surface-molecule interactions. Lateral intermolecular interactions between conjugated organic molecules which can work on noble metal surfaces are classified as follows:

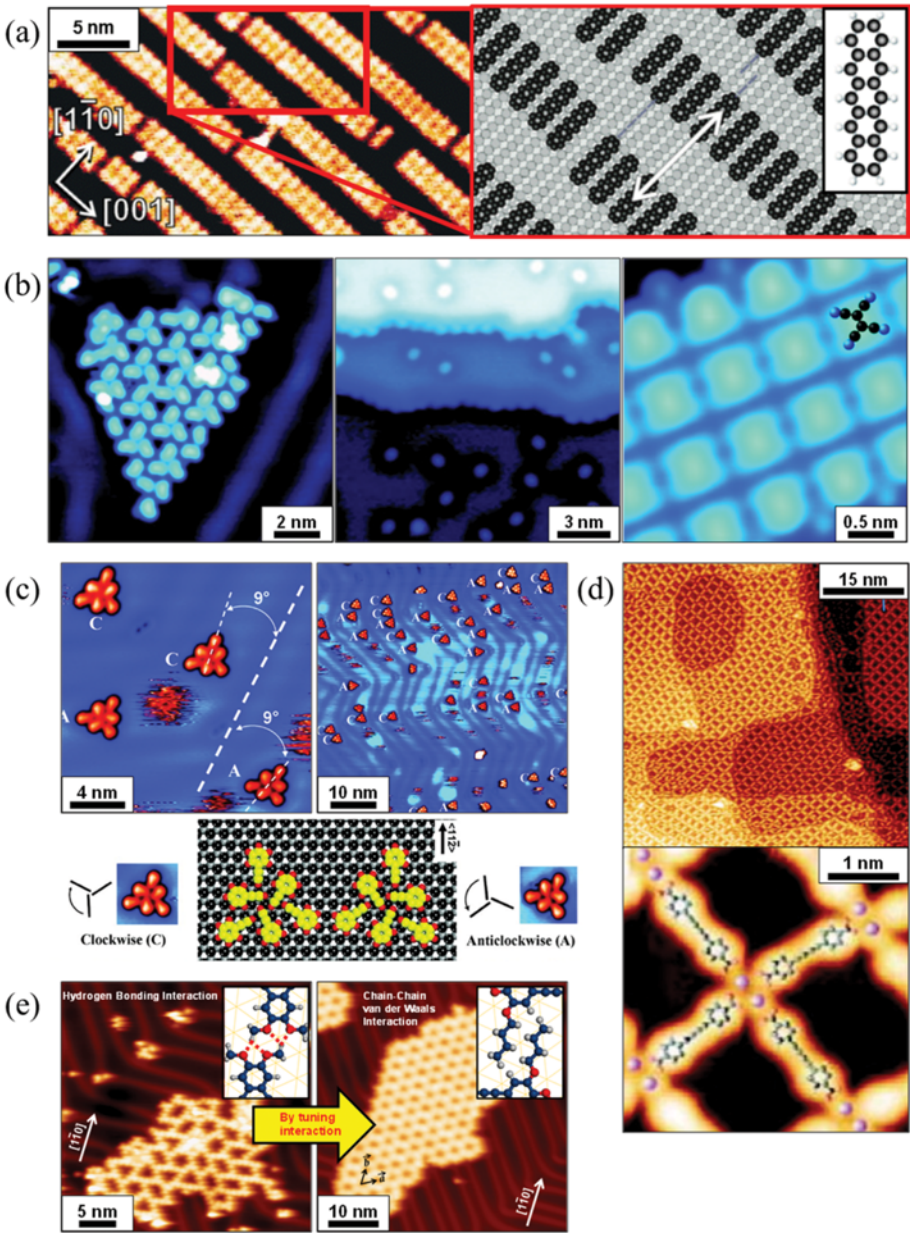

Fig. 6. (a) STM image of pentacene on Cu(110) surface (left) and corresponding model structure (right). The substrate-mediated intermolecular repulsion results in the molecular stripes of pentacene with a long-range ordering. Reprinted with permission from ref. 90; Copyright (2002) American Physical Society. (b) STM images of tetracyanoethylene on Au(111) (left), Ag(100) (middle), and Cu(100) (right). Degree of surface-induced polarity according to work-function of metal and lattice-matching properties changes distribution of the molecules. Reprinted with permission from ref. 97; Copyright (2008) American Chemical Society. (c) STM images of phenylacetylene on Au(111), and hexamer model structures of the molecules exhibiting 2D organizational chirality. Clockwise (C) and anticlockwise (A) chirality of the hexamers are shown in the STM images, and configuration of the hexamers clearly indicates sufficient CH···π interactions. Reprinted with permission from ref. 108; Copyright (2012) American Chemical Society. (d) STM images of 2D metal-organic coordination network on Ag(100) achieved using 4,4′-di-(1,4-buta-1,3-diynyl)-benzoic acid and iron adatoms with ratio of 1 : 1 (upper), and a network structure with the central di-iron binding motif on Au(111) (lower). Reprinted with permission from ref. 112; Copyright (2012) American Chemical Society. (e) STM images of 2D molecular networks formed by the DBA derivatives with methoxy groups (left) and butoxy groups (right), respectively. The intermolecular hydrogen bonding and vdW interactions are tuned by substituting the alkoxy groups, leading to enhancement of the homogeneity of spatial and size distributions. Reprinted with permission from ref. 120; Copyright (2012) American Chemical Society.

I. Substrate-mediated intermolecular repulsion between adsorbed molecules is valid over comparatively long distances [90-94]. A two-dimensional (2D) electron gas state of the metal surface is modulated by the presence of molecules, inducing an indirect intermolecular repulsion (see Fig. 6(a)). This phenomenon implies that the indirect interaction mediated by the metal surface can be strong

enough to effect lateral intermolecular interactions between the adsorbed molecules. Representative instances which fit into this category are behaviors of anthraquinone and pentacene on noble metal surfaces [90-93].

II. Through charge transfer or redistribution of electron density at the O/M interfaces, adsorbed molecules can be charged or have an induced dipole moment in the surface-normal direction [25,64, 65,95,96]. The nature and degree of surface-induced polarity can be varied according to work-function of metal and lattice-matching properties even if identical molecules are adsorbed on noble metal surfaces [97]. Such surface-induced polarity of conjugated organic molecule can interact with neighboring molecules, which significantly contributes to the distribution of molecules on noble metal surfaces (see Fig. 6(b)) [97-102].

III. Conjugated organic molecules with polar groups can exhibit molecular dipoles and/or quadrupoles in the surface plane corresponding to properties of the polar groups, which can play a decisive role in ordering of adsorbed molecules. Hydrogen bonding induced by various functional groups (such as alcohols, carboxylic acids and other hydrogen-donor groups) is one of the most representative instances in this type of interaction, which provides an efficient way to achieve the formation of very homogeneous patterned films and templates [89,93,103-106]. Note that π-conjugation of molecules solely can contribute to hydrogen bonding indirectly, because nodes exist in the plane in which hydrogen bonding occurs [107]. Electronic states of π-conjugated systems thus support the hydrogen bonding interactions. It was recently revealed that even π-conjugated hydrocarbon molecules (i.e., composed of only carbon and hydrogen atoms) can weakly interact with each other via CH$\cdots\pi$ interactions (see Fig. 6(c)) [108].

IV. When metal adatoms are available, adsorbed organic molecules can form metal-organic coordination bonds with the adatoms on the surface (see Fig. 6(d)) [109-113]. In this case, bonding properties are mostly determined by both ligands and metal adatoms employed in the system, and the underlying metal surface also can affect metal-coordination centers via charge transfer [114, 115]. This system is expected to provide benefits in the fields of 2D network design and catalysts.

V. Although vdW interactions intrinsically exist in all cases, more enhanced and specified vdW interactions can be intentionally employed in molecular ordering to maximize 2D crystallization energy [116-119]. It has been demonstrated that the nature of intermolecular interactions in the formation of molecular ordering changes from hydrogen bonding interactions to chain-chain vdW interactions (i.e., chain interdigitation) as the chain length of peripheral alkoxy group increases (see Fig. 6(e)) [120].

Covalent bond formation and polymerization between adsorbed organic molecules are not addressed here, because they are far more related to chemical reactions than interfacial interactions. Fundamentals of such reactions have been reviewed elsewhere [21,121-124].

ELECTRONIC STATES AT ORGANIC-METAL INTERFACES

The nature of electronic states at the O/M interfaces originates from the interactions between highly dispersive states of the metal substrate and rather localized molecular states [40,125-131]. Thus, careful experimental and theoretical approaches are necessarily required to study and understand effects of molecular layers on the surface states of noble metals (e.g., the Shockley surface states) as regards dispersive interface states [132-134].

1. Metal Surface States Observed Through Organic Thin Films

When conjugated organic molecules weakly adsorb (or physisorb) on noble metal surfaces, the metal surface states are normally identified through weakly adsorbed molecular layers. It indicates that weakly adsorbed molecular layers on noble metal surfaces do not quench the surface electronic states of substrates. In this case, highly dispersive surface states of metals are distinctly observed through organic thin films by means of STS or angle-resolved photoemission spectroscopy, which are naturally described as 2D electron gas states, i.e., free-electron-like states [54,135-140]. Interfacial electrons near the E_F are mostly confined to the surface of the metal underneath and highly overlapped with the electronic states of the clean metal surface. Thus, well-defined systems of insulating layers on noble metal surfaces provide deeper insights into weakly adsorbed organic thin films, due to the following similarities near the E_F: (i) two different media exist in one system, i.e., metal/insulator or metal/organic thin film, and (ii) the interface between the two media is electronically transparent and smooth. Particularly in the case of NaCl/Cu(111), an analysis of standing-wave patterns observed through the insulating NaCl layer successfully reveals the electronic states and their physical properties at the metal-insulator interface [141]. As shown in Fig. 7, a one-dimensional (1D) band gap is formed in the 2D electron gas of the interface state band, mostly originating from the surface states of Cu(111), according to growth pattern of the NaCl layer. In addition, refraction of standing waves as well as reflection occurs at the boundaries of NaCl (see Fig. 7(b), (c)). Analogous phenomena to NaCl/Cu(111) are also observed at the interfaces between weakly adsorbed molecular layers and noble metal surfaces. For instance, the molecular layer of bis[1,2,5]thiadiazolotetracyanoquinodimethane (BTDA-TCNQ) on the Au(111) surface exhibits strong and continuous standing waves between the two media near the E_F as shown in Fig. 7(f) [142]. On the other hand, the molecular orbital states of BTDA-TCNQ within the molecular layers are localized independently of the metal surface states (see Fig. 7(g), (h)). Strongly scattered standing waves are thus observed near the boundaries of the molecular layers in the energy regions corresponding to the molecular orbital states (above the E_F), which originate from the reflection of the surface-state electrons at the boundaries. The observation of the scattered surface-state electrons implies that the localized molecular orbital states serve as potential walls for reflecting the surface-state electrons [143].

2. Mixed States of Conjugated Organic Molecules and Noble Metal Surfaces

If molecular adsorption involves chemical interactions with a noble metal surface, valid surface-molecule interactions mainly contribute to determination of the electronic states at the interface and the degree of electron delocalization within the molecular layer. Recent studies show that highly dispersive states at the O/M interfaces can be achieved via strong surface-mediated intermolec-

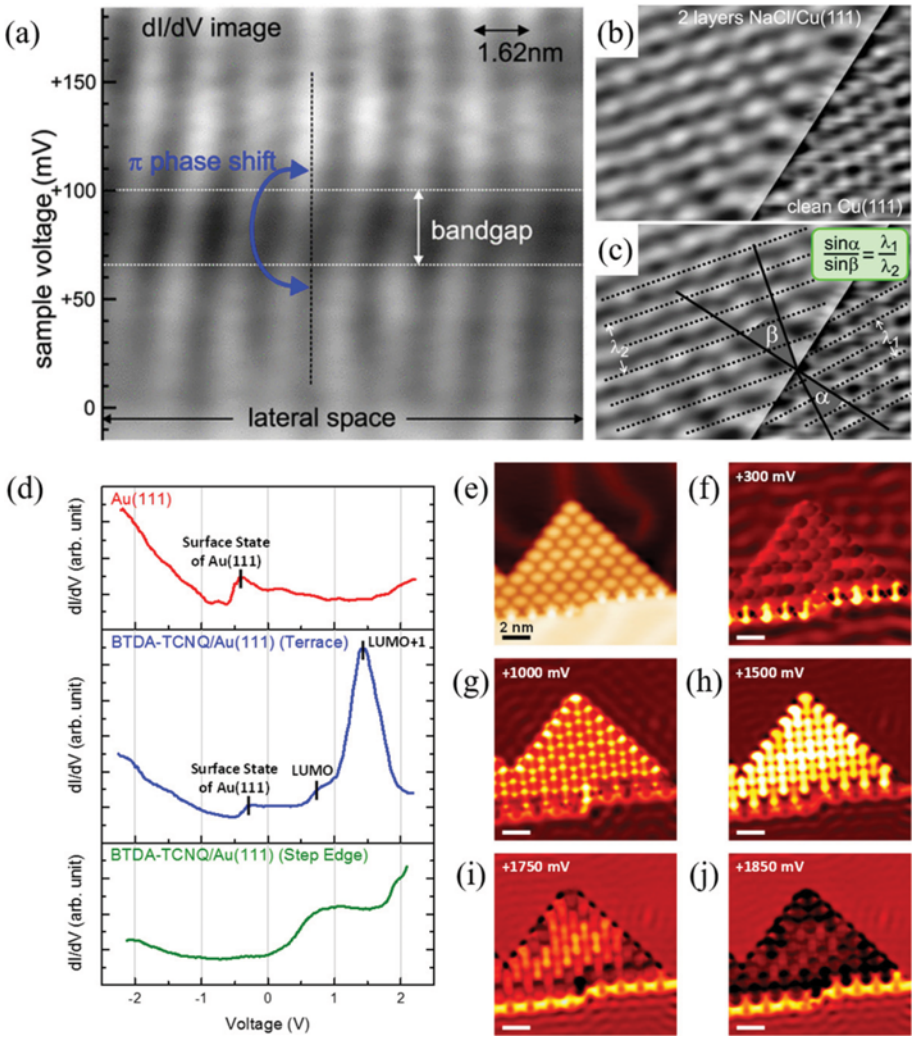

Fig. 7. (a) Spatially resolved STS mapping image of NaCl/Cu(111), showing the probability distribution of the surface electrons in real space and energy. (b) STS mapping image of a NaCl island step edge on Cu(111), showing strong standing-wave patterns on both NaCl and Cu(111) surfaces. (c) Guide lines are added in (b), indicating that the standing-wave patterns satisfy Snell's refraction law. Reprinted with permission from ref. 141; Copyright (2004) American Physical Society. (d) STS spectra of the clean Au(111) surface (top), BTDA-TCNQ on the Au(111) terrace (middle) and BTDA-TCNQ at the Au(111) step edge (bottom). (e) STM image of a molecular island of BTDA-TCNQ on Au(111). (f)-(j) STS mapping images over the same surface area as that in (e), in different energy regions (+300 mV, +1000 mV, +1500 mV, +1750 mV and +1850 mV with respect to the E_F, respectively). Adapted from ref. 142.

ular couplings [144-149]. As shown in Fig. 8, the epitaxial PTCDA/Ag(111) interface has a delocalized 2D band structure which can be identified by the STS experiments [144]. The resonance structures of a confined electron state (n=1, 2, 3) within the molecular layer are clearly revealed in this system and described as a 2D particle-in-a-box model. The free-electron dispersion parabola can be obtained by plotting the dispersion relation, E(k), directly (see Fig. 8(c)). Such delocalized and quantum-confined electronic states at the O/M interfaces exhibit striking similarities with graphene nanostructures on metal surfaces as shown in Fig. 8(d) [150-153]. The observed free-electron band structure mainly originates from the Shockley surface state being dramatically shifted up in energy by interactions with the molecular layer, which is also confirmed by two-photon photoemission (2PPE) spectroscopy and theoretical calculations [146,149]. Similarly, Gonzalez-Lakunza et al. reported that a dispersive hybrid band structure can be achieved at the interface between the organic charge-transfer complexes and the Au surface [148].

Interestingly, the two different types of the electronic states can coexist in one system corresponding to the local position of the system [142]. In case of BTDA-TCNQ/Au(111), the metal surface states are clearly observed on the Au(111) terrace as discussed above. However, at the step edge of Au(111), the molecules show rather strong interactions with the surface. Substantial broadening of the unoccupied molecular states is induced by hybridization with the electronic states of the metal surface at the step edge, and thus the step-edge states of Au(111) and the molecular states are not distinguishable with the STS experiments (see Fig. 7(d)). Such locally mixed states originate from the step dipole described as the Smoluchowski effect [134,154,155]. Since the step dipole has an

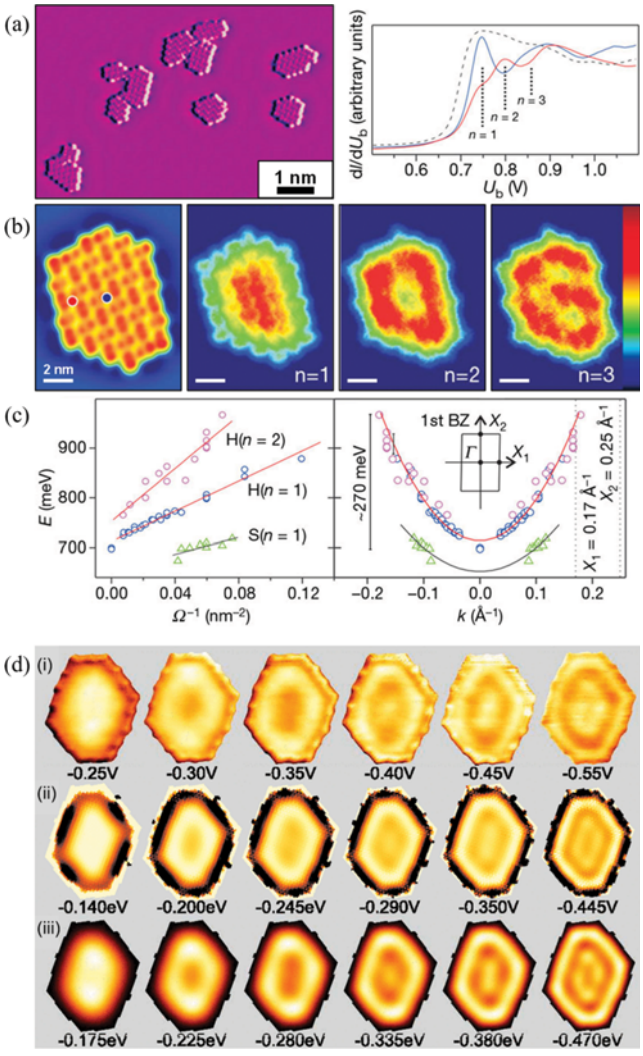

Fig. 8. (a) STM image of small molecular islands of PTCDA/Ag(111) (left), and STS spectra of PTCDA/Ag(111) presented in (b). Red and blue lines are STS spectra measured on spots marked with red and blue circles in (b), respectively, and first three confined states are also indicated with vertical dotted lines. Dashed line corresponds to the monolayer spectrum of PTCDA/Ag(111). (b) STM image and STS mapping images at first three confined states (+750 mV, +800 mV and +860 mV with respect to the E_F, respectively) of a molecular island of PTCDA on Ag(111). (c) Energy of the confined states versus inverse island area for the herringbone (H) and square (S) phase islands of PTCDA/Ag(111) (left), and their parabolic dispersion mirrored at k=0 (right). Reprinted with permission from ref. 144; Copyright (2006) Nature Publishing Group. (d) (i) STS mapping images of graphene quantum dots on Ir(111), and (ii, iii) corresponding local density of states calculated using a tight-binding model (ii) and the Klein-Gordon equation (iii), respectively, in different energy regions as indicated in the figure with respect to the E_F. Reprinted with permission from ref. 150; Copyright (2011) American Physical Society.

opposite direction to the surface dipole, a strong localized electric field is induced at the step edge. It results in Stark shifts of the adsorbates near the step edge, and thus the charge is partially transferred only from the step edge to the unoccupied molecular states. Consequently, the unoccupied molecular states of the BTDA-TCNQ molecules are highly hybridized with the Au surface at the step edge, forming quasi-1D electron dispersion along the step-edge line as shown in Fig. 7(i), (j).

CONCLUSION AND FUTURE PERSPECTIVES

The main purpose of this review is to provide a better understanding of interfacial contacts between conjugated organic molecules and noble metal surfaces, and methodology to control interfacial interactions and their related phenomena. Advantages of noble metals can be highlighted as follows: (i) noble metals have been widely used as electrodes in molecule-based electronics owing to their chemical inertness, differently from other transition metals which cause oxidation or instability, (ii) the use of noble metal substrates facilitates control of surface-molecule interactions corresponding to work-function of metal, surface lattice and surface templating effect, and (iii) intentional tuning of intermolecular interactions at the O/M interfaces can be achieved by careful design of molecules incorporating chemical properties, because conjugated organic molecules normally lie flat on noble metal surfaces. In addition, molecular orientation, alignment and ordering on the electrodes have profound effects on the electrical and optical properties of organic electronic and optoelectronic devices [2,156]. This review covers only a limited range from single molecules to submonolayer molecular films on noble metal surfaces. However, as probed through extensively performed studies, the fact that interfacial interactions have strong correlation with geometric and electronic structures of the entire system as well as single adsorption events imbues this review with special significance in molecule-based electronics. I anticipate that this review will provide not only a deeper insight into interfacial contacts, but also a general basis for designing the architecture of molecule-based electronics for future applications.

ACKNOWLEDGEMENTS

This work was supported by Basic Science Research Program through the National Research Foundation of Korea (No. NRF-2015R1D1A1A01060089).

REFERENCES

1. A. J. Heeger, S. Kivelson, J. R. Schrieffer and W. P. Su, *Rev. Mod. Phys.*, **60**, 781 (1988).
2. C. D. Dimitrakopoulos and P. R. Malenfant, *Adv. Mater.*, **14**, 99 (2002).
3. J. R. Heath and M. A. Ratner, *Phys. Today*, **56**, 43 (2003).
4. S. R. Forrest, *Nature*, **428**, 911 (2004).
5. M. Berggren and A. Richter-Dahlfors, *Adv. Mater.*, **19**, 3201 (2007).
6. X.-Y. Zhu, *Surf. Sci. Rep.*, **56**, 1 (2004).
7. C. W. Tang, *Appl. Phys. Lett.*, **48**, 183 (1986).
8. C. W. Tang and S. A. VanSlyke, *Appl. Phys. Lett.*, **51**, 913 (1987).
9. D. Braun and A. J. Heeger, *Appl. Phys. Lett.*, **58**, 1982 (1991).
10. G. Yu, J. Gao, J. C. Hummelen, F. Wudl and A. J. Heeger, *Science*,

270, 1789 (1995).
11. A. Nitzan and M. A. Ratner, *Science*, **300**, 1384 (2003).
12. P. Peumans, S. Uchida and S. R. Forrest, *Nature*, **425**, 158 (2003).
13. P. Peumans, A. Yakimov and S. R. Forrest, *J. Appl. Phys.*, **93**, 3693 (2003).
14. B. W. D'Andrade and S. R. Forrest, *Adv. Mater.*, **16**, 1585 (2004).
15. S. R. Forrest, *MRS Bull.*, **30**, 28 (2005).
16. P. Hänggi and F. Marchesoni, *Rev. Mod. Phys.*, **81**, 387 (2009).
17. H. Uoyama, K. Goushi, K. Shizu, H. Nomura and C. Adachi, *Nature*, **492**, 234 (2012).
18. D. J. Beesley, J. Semple, L. K. Jagadamma, A. Amassian, M. A. McLachlan and T. D. Anthopoulos, *Nat. Commun.*, **5**, 3933 (2014).
19. S. R. Forrest, *Chem. Rev.*, **97**, 1793 (1997).
20. J. V. Barth, G. Costantini and K. Kern, *Nature*, **437**, 671 (2005).
21. L. Bartels, *Nat. Chem.*, **2**, 87 (2010).
22. H. Ishii, K. Sugiyama, E. Ito and K. Seki, *Adv. Mater.*, **11**, 605 (1999).
23. H. Yamane, K. Kanai, Y. Ouchi, N. Ueno and K. Seki, *J. Electron. Spectrosc. Relat. Phenom.*, **174**, 28 (2009).
24. B. Hammer and J. Norskov, *Nature*, **376**, 238 (1995).
25. F. Tautz, *Prog. Surf. Sci.*, **82**, 479 (2007).
26. J. P. P. Ramalho, J. R. B. Gomes and F. Illas, *RSC Adv.*, **3**, 13085 (2013).
27. D. A. Egger, Z. F. Liu, J. B. Neaton and L. Kronik, *Nano Lett.*, **15**, 2448 (2015).
28. R. Wisendanger, *Scanning probe microscopy and spectroscopy: Methods and applications*, Cambridge University Press, New York (1994).
29. G. Binnig, H. Rohrer, C. Gerber and E. Weibel, *Appl. Phys. Lett.*, **40**, 178 (1982).
30. G. Binnig, H. Rohrer, C. Gerber and E. Weibel, *Phys. Rev. Lett.*, **50**, 120 (1983).
31. G. Binnig and H. Rohrer, *Rev. Mod. Phys.*, **59**, 615 (1987).
32. R. Hamers, *Annu. Rev. Phys. Chem.*, **40**, 531 (1989).
33. R. Becker, J. A. Golovchenko, D. Hamann and B. Swartzentruber, *Phys. Rev. Lett.*, **55**, 2032 (1985).
34. G. Binnig, K. Frank, H. Fuchs, N. Garcia, B. Reihl, H. Rohrer, F. Salvan and A. Williams, *Phys. Rev. Lett.*, **55**, 991 (1985).
35. G. Binnig, N. Garcia and H. Rohrer, *Phys. Rev. B*, **32**, 1336 (1985).
36. L. W. Bruch, *Surf. Sci.*, **125**, 194 (1983).
37. R. Hoffmann, *Rev. Mod. Phys.*, **60**, 601 (1988).
38. S. M. Barlow and R. Raval, *Surf. Sci. Rep.*, **50**, 201 (2003).
39. V. Humblot, S. M. Barlow and R. Raval, *Prog. Surf. Sci.*, **76**, 1 (2004).
40. C. D. Lindstrom and X. Y. Zhu, *Chem. Rev.*, **106**, 4281 (2006).
41. X. Crispin, V. Geskin, A. Crispin, J. Cornil, R. Lazzaroni, W. R. Salaneck and J.-L. Brédas, *J. Am. Chem. Soc.*, **124**, 8131 (2002).
42. S. Braun, W. R. Salaneck and M. Fahlman, *Adv. Mater.*, **21**, 1450 (2009).
43. J. W. M. Frenken and P. Stoltze, *Phys. Rev. Lett.*, **82**, 3500 (1999).
44. H. L. Skriver and N. M. Rosengaard, *Phys. Rev. B*, **45**, 9410 (1992).
45. H. L. Skriver and N. M. Rosengaard, *Phys. Rev. B*, **46**, 7157 (1992).
46. D. E. Hooks, T. Fritz and M. D. Ward, *Adv. Mater.*, **13**, 227 (2001).
47. W. Chen, V. Madhavan, T. Jamneala and M. Crommie, *Phys. Rev. Lett.*, **80**, 1469 (1998).
48. M. Bohringer, K. Morgenstern, W. D. Schneider, M. Wuhn, C. Woll and R. Berndt, *Surf. Sci.*, **444**, 199 (2000).
49. S. Clair, S. Pons, H. Brune, K. Kern and J. V. Barth, *Angew. Chem. Int. Ed. Engl.*, **44**, 7294 (2005).
50. F. Silly, A. Q. Shaw, G. A. D. Briggs and M. R. Castell, *Appl. Phys. Lett.*, **92**, 023102 (2008).
51. P. Maksymovych and D. B. Dougherty, *Surf. Sci.*, **602**, 2017 (2008).
52. P. Han, B. A. Mantooth, E. C. H. Sykes, Z. J. Donhauser and P. S. Weiss, *J. Am. Chem. Soc.*, **126**, 10787 (2004).
53. P. G. Schroeder, C. B. France, J. B. Park and B. A. Parkinson, *J. Appl. Phys.*, **91**, 3010 (2002).
54. Y. J. Song, K. Lee, S. H. Kim, B.-Y. Choi, J. Yu and Y. Kuk, *Nano Lett.*, **10**, 996 (2010).
55. T. Komeda, H. Isshiki and J. Liu, *Sci. Technol. Adv. Mater.*, **11**, 054602 (2010).
56. B. A. Mantooth, E. C. H. Sykes, P. Han, A. M. Moore, Z. J. Donhauser, V. H. Crespi and P. S. Weiss, *J. Phys. Chem. C*, **111**, 6167 (2007).
57. J. Kang and X.-Y. Zhu, *Chem. Mater.*, **18**, 1318 (2006).
58. C. Seidel, R. Ellerbrake, L. Gross and H. Fuchs, *Phys. Rev. B*, **64**, 195418 (2001).
59. K. Manandhar, J. B. Sambur and B. A. Parkinson, *J. Appl. Phys.*, **107**, 063716 (2010).
60. J.-H. Kim, J. Jung, K. Tahara, Y. Tobe, Y. Kim and M. Kawai, *J. Chem. Phys.*, **140**, 074709 (2014).
61. A. Kahn, N. Koch and W. Gao, *J. Polym. Sci., Part B: Polym. Phys.*, **41**, 2529 (2003).
62. G. Witte, S. Lukas, P. S. Bagus and C. Woll, *Appl. Phys. Lett.*, **87**, 263502 (2005).
63. K. Glöckler, C. Seidel, A. Soukopp, M. Sokolowski, E. Umbach, M. Böhringer, R. Berndt and W.-D. Schneider, *Surf. Sci.*, **405**, 1 (1998).
64. M. Eremtchenko, J. Schaefer and F. Tautz, *Nature*, **425**, 602 (2003).
65. A. Hauschild, K. Karki, B. C. C. Cowie, M. Rohlfing, F. S. Tautz and M. Sokolowski, *Phys. Rev. Lett.*, **94**, 036106 (2005).
66. Y. Zou, L. Kilian, A. Schöll, T. Schmidt, R. Fink and E. Umbach, *Surf. Sci.*, **600**, 1240 (2006).
67. N. Lorente, M. F. G. Hedouin, R. E. Palmer and M. Persson, *Phys. Rev. B*, **68**, 155401 (2003).
68. A. Ferretti, C. Baldacchini, A. Calzolari, R. Di Felice, A. Ruini, E. Molinari and M. G. Betti, *Phys. Rev. Lett.*, **99**, 046802 (2007).
69. J. Gottschalck and B. Hammer, *J. Chem. Phys.*, **116**, 784 (2002).
70. P. Maksymovych, D. C. Sorescu and J. T. Yates, *Phys. Rev. Lett.*, **97**, 146103 (2006).
71. K. Toyoda, Y. Nakano, I. Hamada, K. Lee, S. Yanagisawa and Y. Morikawa, *Surf. Sci.*, **603**, 2912 (2009).
72. K. Toyoda, I. Hamada, K. Lee, S. Yanagisawa and Y. Morikawa, *J. Chem. Phys.*, **132**, 134703 (2010).
73. M. Kind and C. Wöll, *Prog. Surf. Sci.*, **84**, 230 (2009).
74. M. Doering, J. Buisset, H.-P. Rust, B. G. Briner and A. M. Bradshaw, *Faraday Discuss.*, **105**, 163 (1996).
75. J. T. Kim, T. Kawai, J. Yoshinobu and M. Kawai, *Surf. Sci.*, **360**, 50 (1996).
76. J. Yoshinobu, H. Tanaka, T. Kawai and M. Kawai, *Phys. Rev. B*, **53**, 7492 (1996).
77. N. D. Lang, *Phys. Rev. Lett.*, **46**, 842 (1981).
78. P. S. Bagus, V. Staemmler and C. Woll, *Phys. Rev. Lett.*, **89**, 096104 (2002).
79. J. K. Nørskov, *Rep. Prog. Phys.*, **53**, 1253 (1990).

80. G. P. Brivio and M. I. Trioni, *Rev. Mod. Phys.*, **71**, 231 (1999).
81. D. M. Newns, *Phys. Rev.*, **178**, 1123 (1969).
82. K. Koyama, N. Yamaguchi and T. Miyasaka, *Science*, **265**, 762 (1994).
83. Z. J. Donhauser, B. A. Mantooth, K. F. Kelly, L. A. Bumm, J. D. Monnell, J. J. Stapleton, D. W. Price Jr., A. M. Rawlett, D. L. Allara, J. M. Tour and P. S. Weiss, *Science*, **292**, 2303 (2001).
84. J. Taylor, M. Brandbyge and K. Stokbro, *Phys. Rev. Bv* **68**, 121101(R) (2003).
85. P. A. Lewis, C. E. Inman, F. Maya, J. M. Tour, J. E. Hutchison and P. S. Weiss, *J. Am. Chem. Soc.*, **127**, 17421 (2005).
86. A. M. Moore, A. A. Dameron, B. A. Mantooth, R. K. Smith, D. J. Fuchs, J. W. Ciszek, F. Maya, Y. Yao, J. M. Tour and P. S. Weiss, *J. Am. Chem. Soc.*, **128**, 1959 (2006).
87. S. M. Lindsay and M. A. Ratner, *Adv. Mater.*, **19**, 23 (2007).
88. J. M. Mativetsky, G. Pace, M. Elbing, M. A. Rampi, M. Mayor and P. Samorì, *J. Am. Chem. Soc.*, **130**, 9192 (2008).
89. Y. Wang, X. Ge, G. Schull, R. Berndt, H. Tang, C. Bornholdt, F. Koehler and R. Herges, *J. Am. Chem. Soc.*, **132**, 1196 (2010).
90. S. Lukas, G. Witte and C. Woll, *Phys. Rev. Lett.*, **88**, 028301 (2002).
91. L. Gavioli, M. Fanetti, M. Sancrotti and M. G. Betti, *Phys. Rev. B*, **72**, 035458 (2005).
92. C. Baldacchini, C. Mariani and M. G. Betti, *J. Chem. Phys.*, **124**, 154702 (2006).
93. G. Pawin, K. L. Wong, K. Y. Kwon and L. Bartels, *Science*, **313**, 961 (2006).
94. F. Vonau, D. Aubel, L. Bouteiller, G. Reiter and L. Simon, *Phys. Rev. Lett.*, **99**, 086103 (2007).
95. Y. Konishi, Y. Sainoo, K. Kanazawa, S. Yoshida, A. Taninaka, O. Takeuchi and H. Shigekawa, *Phys. Rev. B*, **71**, 193410 (2005).
96. L. Zoppi, A. Garcia and K. K. Baldridge, *J. Phys. Chem. A*, **114**, 8864 (2010).
97. D. Wegner, R. Yamachika, Y. Wang, V. W. Brar, B. M. Bartlett, J. R. Long and M. F. Crommie, *Nano Lett.*, **8**, 131 (2008).
98. I. Fernandez-Torrente, S. Monturet, K. J. Franke, J. Fraxedas, N. Lorente and J. I. Pascual, *Phys. Rev. Lett.*, **99**, 176103 (2007).
99. T. Bauert, L. Merz, D. Bandera, M. Parschau, J. S. Siegel and K. H. Ernst, *J. Am. Chem. Soc.*, **131**, 3460 (2009).
100. L. Merz, M. Parschau, L. Zoppi, K. K. Baldridge, J. S. Siegel and K. H. Ernst, *Angew. Chem. Int. Ed. Engl.*, **48**, 1966 (2009).
101. O. Guillermet, E. Niemi, S. Nagarajan, X. Bouju, D. Martrou, A. Gourdon and S. Gauthier, *Angew. Chem. Int. Ed. Engl.*, **48**, 1970 (2009).
102. T.-C. Tseng, C. Urban, Y. Wang, R. Otero, S. L. Tait, M. Alcamí, D. Écija, M. Trelka, J. M. Gallego and N. Lin, *Nat. Chem.*, **2**, 374 (2010).
103. J. V. Barth, J. Weckesser, C. Z. Cai, P. Gunter, L. Burgi, O. Jeandupeux and K. Kern, *Angew. Chem. Int. Ed. Engl.*, **39**, 1230 (2000).
104. J. M. MacLeod, O. Ivasenko, C. Fu, T. Taerum, F. Rosei and D. F. Perepichka, *J. Am. Chem. Soc.*, **131**, 16844 (2009).
105. H. W. Kim, J. Jung, M. Han, S. Lim, K. Tamada, M. Hara, M. Kawai, Y. Kim and Y. Kuk, *J. Am. Chem. Soc.*, **133**, 9236 (2011).
106. J. A. Theobald, N. S. Oxtoby, M. A. Phillips, N. R. Champness and P. H. Beton, *Nature*, **424**, 1029 (2003).
107. K. Y. Kwon, G. Pawin, K. L. Wong, E. Peters, D. Kim, S. Hong, T. S. Rahman, M. Marsella and L. Bartels, *J. Am. Chem. Soc.*, **131**, 5540 (2009).
108. Q. Li, C. B. Han, S. R. Horton, M. Fuentes-Cabrera, B. G. Sumpter, W. C. Lu, J. Bernholc, P. Maksymovych and M. H. Pan, *ACS Nano*, **6**, 566 (2012).
109. A. Dmitriev, H. Spillmann, N. Lin, J. V. Barth and K. Kern, *Angew. Chem. Int. Ed. Engl.*, **42**, 2670 (2003).
110. U. Schlickum, R. Decker, F. Klappenberger, G. Zoppellaro, S. Klyatskaya, M. Ruben, I. Silanes, A. Arnau, K. Kern, H. Brune and J. V. Barth, *Nano Lett.*, **7**, 3813 (2007).
111. D. Kuhne, F. Klappenberger, R. Decker, U. Schlickum, H. Brune, S. Klyatskaya, M. Ruben and J. V. Barth, *J. Am. Chem. Soc.*, **131**, 3881 (2009).
112. C. S. Kley, J. Čechal, T. Kumagai, F. Schramm, M. Ruben, S. Stepanow and K. Kern, *J. Am. Chem. Soc.*, **134**, 6072 (2012).
113. Y. Li, J. Xiao, T. E. Shubina, M. Chen, Z. Shi, M. Schmid, H.-P. Steinrück, J. M. Gottfried and N. Lin, *J. Am. Chem. Soc.*, **134**, 6401 (2012).
114. N. Abdurakhmanova, A. Floris, T.-C. Tseng, A. Comisso, S. Stepanow, A. De Vita and K. Kern, *Nat. Commun.*, **3**, 940 (2012).
115. A. Floris, A. Comisso and A. De Vita, *ACS Nano*, **7**, 8059 (2013).
116. X. Qiu, C. Wang, Q. Zeng, B. Xu, S. Yin, H. Wang, S. Xu and C. L. Bai, *J. Am. Chem. Soc.*, **122**, 5550 (2000).
117. S. Xu, Q. Zeng, J. Lu, C. Wang, L. Wan and C. L. Bai, *Surf. Sci.*, **538**, L451 (2003).
118. L. Merz, H.-J. Güntherodt, L. J. Scherer, E. C. Constable, C. E. Housecroft, M. Neuburger and B. A. Hermann, *Chem. Eur. J.*, **11**, 2307 (2005).
119. S. Ahn, C. N. Morrison and A. J. Matzger, *J. Am. Chem. Soc.*, **131**, 7946 (2009).
120. J.-H. Kim, K. Tahara, J. Jung, S. De Feyter, Y. Tobe, Y. Kim and M. Kawai, *J. Phys. Chem. C*, **116**, 17082 (2012).
121. M. Xi and B. E. Bent, *J. Am. Chem. Soc.*, **115**, 7426 (1993).
122. L. Grill, M. Dyer, L. Lafferentz, M. Persson, M. V. Peters and S. Hecht, *Nat. Nanotechnol.*, **2**, 687 (2007).
123. N. A. A. Zwaneveld, R. Pawlak, M. Abel, D. Catalin, D. Gigmes, D. Bertin and L. Porte, *J. Am. Chem. Soc.*, **130**, 6678 (2008).
124. A. Gourdon, *Angew. Chem. Int. Ed. Engl.*, **47**, 6950 (2008).
125. R. L. Lingle, D. F. Padowitz, R. E. Jordan, J. D. Mcneill and C. B. Harris, *Phys. Rev. Lett.*, **72**, 2243 (1994).
126. C. B. Harris, N. H. Ge, R. L. Lingle, J. D. McNeill and C. M. Wong, *Annu. Rev. Phys. Chem.*, **48**, 711 (1997).
127. G. Dutton and X. Y. Zhu, *J. Phys. Chem. B*, **105**, 10912 (2001).
128. M. Muntwiler, C. D. Lindstrom and X. Y. Zhu, *J. Chem. Phys.*, **124**, 081104 (2006).
129. K. Schouteden, P. Lievens and C. Van Haesendonck, *Phys. Rev. B*, **79**, 195409 (2009).
130. K. M. Andrews and T. P. Pearl, *J. Chem. Phys.*, **132**, 214701 (2010).
131. M. Ternes, M. Pivetta, F. Patthey and W. D. Schneider, *Prog. Surf. Sci.*, **85**, 1 (2010).
132. W. Shockley, *Phys. Rev.*, **56**, 317 (1939).
133. L. Davis, M. Everson, R. Jaklevic and W. Shen, *Phys. Rev. B*, **43**, 3821 (1991).
134. P. Avouris, I.-W. Lyo and P. Molinas-Mata, *Chem. Phys. Lett.*, **240**, 423 (1995).
135. A. C. Dürr, N. Koch, M. Kelsch, A. Rühm, J. Ghijsen, R. L. Johnson, J.-J. Pireaux, J. Schwartz, F. Schreiber, H. Dosch and A.

Kahn, *Phys. Rev. B*, **68**, 115428 (2003).
136. N. Nicoara, E. Román, J. M. Gómez-Rodríguez, J. A. Martín-Gago and J. Méndez, *Org. Electron.*, **7**, 287 (2006).
137. E. Kawabe, H. Yamane, R. Sumii, K. Koizumi, Y. Ouchi, K. Seki and K. Kanai, *Org. Electron.*, **9**, 783 (2008).
138. I. F. Torrente, K. J. Franke and J. I. Pascual, *Int. J. Mass Spectrom.*, **277**, 269 (2008).
139. J. Ziroff, P. Gold, A. Bendounan, F. Forster and F. Reinert, *Surf. Sci.*, **603**, 354 (2009).
140. W.-H. Soe, C. Manzano, A. De Sarkar, N. Chandrasekhar and C. Joachim, *Phys. Rev. Lett.*, **102**, 176102 (2009).
141. J. Repp, G. Meyer and K.-H. Rieder, *Phys. Rev. Lett.*, **92**, 036803 (2004).
142. J.-H. Kim, J.-C. Ribierre, Y. S. Yang, C. Adachi, M. Kawai, J. Jung, T. Fukushima and Y. Kim, *Nat. Commun.*, **7**, 10653 (2016).
143. L. Gross, F. Moresco, L. Savio, A. Gourdon, C. Joachim and K.-H. Rieder, *Phys. Rev. Lett.*, **93** (2004).
144. R. Temirov, S. Soubatch, A. Luican and F. Tautz, *Nature*, **444**, 350 (2006).
145. K. Kanazawa, Y. Sainoo, Y. Konishi, S. Yoshida, A. Taninaka, A. Okada, M. Berthe, N. Kobayashi, O. Takeuchi and H. Shigekawa, *J. Am. Chem. Soc.*, **129**, 740 (2007).
146. C. H. Schwalb, S. Sachs, M. Marks, A. Scholl, F. Reinert, E. Umbach and U. Hofer, *Phys. Rev. Lett.*, **101**, 146801 (2008).
147. M. S. Dyer and M. Persson, *J. Phys.: Condens. Matter*, **20**, 312002 (2008).
148. N. Gonzalez-Lakunza, I. Fernandez-Torrente, K. Franke, N. Lorente, A. Arnau and J. Pascual, *Phys. Rev. Lett.*, **100**, 156805 (2008).
149. M. S. Dyer and M. Persson, *New J. Phys.*, **12**, 063014 (2010).
150. S. K. Hamalainen, Z. X. Sun, M. P. Boneschanscher, A. Uppstu, M. Ijas, A. Harju, D. Vanmaekelbergh and P. Liljeroth, *Phys. Rev. Lett.*, **107**, 236803 (2011).
151. S. H. Phark, J. Borme, A. L. Vanegas, M. Corbetta, D. Sander and J. Kirschner, *ACS Nano*, **5**, 8162 (2011).
152. D. Subramaniam, F. Libisch, Y. Li, C. Pauly, V. Geringer, R. Reiter, T. Mashoff, M. Liebmann, J. Burgdorfer, C. Busse, T. Michely, R. Mazzarello, M. Pratzer and M. Morgenstern, *Phys. Rev. Lett.*, **108**, 046801 (2012).
153. H. W. Kim, S. Takemoto, E. Minamitani, T. Okada, T. Takami, K. Motobayashi, M. Trenary, M. Kawai, N. Kobayashi and Y. Kim, *J. Phys. Chem. C*, **120**, 345 (2015).
154. K. Wandelt, *Surf. Sci.*, **251**, 387 (1991).
155. M. Kamna, S. Stranick and P. Weiss, *Isr. J. Chem.*, **36**, 59 (1996).
156. D. Yokoyama, *J. Mater. Chem.*, **21**, 19187 (2011).

Ju-Hyung Kim received the B.S. and M.S. degrees in chemical and biological engineering from Seoul National University, Korea, in 2007, and the Ph.D. degree in advanced materials science from the University of Tokyo, Japan, in 2012, working on organic semiconductors and organic/metal interfaces. From 2009 to 2012, he was an International Program Associate (IPA) Research Fellow of RIKEN, Japan. He also performed postdoctoral work at Center for Organic Photonics and Electronics Research (OPERA), Kyushu University, Japan, and served as an Assistant Professor at Pukyong National University, Korea. Since 2016, he has been an Assistant Professor of Chemical Engineering at Ajou University, Korea. His research interest includes organic electronic/optoelectronic applications, unconventional lithography methodology, surface engineering and analysis on organic thin films.